RSC Advances

ROYAL SOCIETY OF CHEMISTRY

www.rsc.org/advances

Total internal reflection Raman spectroscopy of poly(alpha-olefin) oils in a lubricated contact

Manimunda Praveena[†], Kaustav Guha[§], Abhilash Ravishankar[‡],Sanjay K. Biswas[‡],

Colin D. Bain[§*] and Vikram Jayaram[†]

[†]Department of Materials Engineering, Indian Institute of Science, Bangalore, India

[‡] Department of Mechanical Engineering, Indian Institute of Science, Bangalore, India

[§] Department of Chemistry, Durham University, Durham, U.K.

Abstract: The rheology of a poly (alpha-olefin) base oil (PAO) in a sliding point contact has been investigated by total internal reflection (TIR) Raman spectroscopy. TIR Raman has the sensitivity to analyse nanometer-thick lubricant film in a tribological contact. The Raman signal generated from the sliding contact was used to determine the lubricant film thickness. The experimentally obtained film thicknesses were compared with theoretical calculations and a transition from Newtonian to non-Newtonian behaviour was observed at high shear rates. The Raman spectra showed no significant changes in the conformation of the PAO chains under the applied conditions of pressure and shear, but the polarisation dependence of the spectra revealed a preferred orientation of the hydrocarbon side chains in the shear-thinned region. Monolayers formed by a boundary lubricant, arachidic acid, dissolved in the PAO could be detected on the surfaces in the elastohydrodynamic regime.

Keywords: TIR Raman, shear thinning, PAO

[*]Corresponding author. E-mail: c.d.bain@durham.ac.uk

1. Introduction

In modern-day industry the demand for high performance lubricants is ever-increasing. Lubricants, such as engine oil, must perform at extreme conditions of pressure and shear over a wide temperature range (–40 °C to 150 °C).[1, 2] The selection of an engine oil is based on the viscosity required to provide adequate lubrication at a given operating temperature. The increase in temperature at loaded bearings or engine components causes a sharp decrease in the viscosity of mineral oils, leading to lower film thickness and enhanced wear of engine components. To maintain the viscosity of the engine oil at operating temperatures, viscosity modifiers – mainly polymers of high molecular weight – are added to mineral oils.[3]

In recent times as a replacement for mineral oils, synthetic oils such as poly(alpha-olefins) (PAO) are used as base oil.[4] Synthetic base oils are having some advantages over mineral oils: they are moderately priced, have high oxidation and thermal stability and have low pour points, and perform well over a wide range of temperatures.[3] At high contact pressure, the lubricant film in a tribological contact experiences severe mechanical stresses. At shear rates above 10^5 s^{-1}, entangled polymer chains start to align in the direction of shear and the result is reflected in a decrease of oil viscosity.[5] This phenomenon is known as shear thinning and the viscosity loss is completely recoverable. When viscosity modifiers are added to mineral oils, the oil starts to shear thin at much lower shear rates ($<10^5$ s^{-1}) and the viscosity drops sharply until it reaches the viscosity of the pure base oil and, with further increase in shear rate, the viscosity remains the same.[6-8] In the EHL lubrication regime, friction determines the power loss in the contact.[9] Shear thinning results in lowering of friction but at the same time a decrease in film thickness leads to the wear of the engine components.[10] From the lubricant engineer's perspective, the

understanding of the rheology of the base oil is crucial. The present work aimed to gain more insights into the complex physiochemical changes associated with shear thinning in synthetic base oil in the absence of viscosity modifiers.

Many researchers have developed theoretical formulations to predict the EHL film thickness, starting with Ertel in 1940.[11] Later, Dowson and Higginson solved the line contact problem and Hamrock and Dowson developed a widely used formula for the central film thickness in a point contact.[11] To validate the theoretical predictions, different experimental techniques were developed.[12] Optical interferometry is one such technique commonly used to measure the oil film thickness.[13-15] The detection limit of optical interferometry was initially limited to ~100 nm. The development of spacer-layer imaging by Johnston *et al.* enabled the detection of very thin (5 nm) lubricant films.[16-18] Using an advanced form of optical interferometry, Spikes *et al*. studied boundary films of oleic acid (2–20 nm thick).[19] However, optical imaging on its own does not give any information on the chemical state or orientation of lubricant molecules. Combining optical imaging with spectroscopy is one way to get information about the chemical state of the molecules. Lauer *et al.* first adapted IR emission spectroscopy to study base stock and additive response in sliding contacts.[20] Cann *et al.* combined optical imaging with IR spectroscopy to study hydrocarbon lubricants within a contact.[21] Raman spectroscopy has also been used to study lubricant films in a tribological contact, but in a normal confocal Raman microscope the sensitivity is marginal for studying sub-100 nm thick films in the EHD regime and inadequate for the study of boundary lubrication.[13, 22-26] The use of a total internal reflection geometry in which the Raman signal is generated from an evanescent wave enhances the Raman signal and permits the detection of ultrathin lubricant films in the contact zone, with a spatial resolution of ~ 10 μm .[27-31]

In this paper, we demonstrate the application of TIR Raman spectroscopy for the *in situ* study of shear thinning in synthetic PAO base oil. The intensity of the Raman spectra is used to determine the fluid film thickness quantitatively and the results compared with the predictions of EHD models. The relative intensities of different C–H stretching modes is used to track any changes in conformation with pressure and shear and the relative intensity of spectra with different polarizations is used to infer the alignment of molecules under shear. Finally, we use TIR Raman spectroscopy to observe the presence of a boundary lubricant on the surfaces in a sheared contact between glass and silica.

2. Experimental

2.1 Materials

The test lubricant used in all the experiments was poly(alpha-olefin), supplied by Chemtura Ltd. U.K. Two different viscosity grades (PAO100 and PAO 40) were used to provide a range of film thickness at low sliding speeds. Arachidic acid and deuterated arachidic acid (Sigma-Aldrich) were used as received.

2.2 **Friction tests**

Friction tests were performed using custom-built, ball-on-flat, Raman tribometer.[31] The normal load and sliding speed varied from 0.5–3 N and 2–10 mm s^{-1}, respectively. A dead weight loading mechanism was used to apply the normal load. The mating bodies were SF10 glass hemisphere (10 mm diameter, Young's modulus, $Y = 64$ GPa) and silica ball (8 mm diameter and $Y = 73$ GPa). Experiments were conducted at ambient humidity (RH ~ 35%) and temperature (T

~ 298 K). The Hertzian contact pressures at the SF10–silica interface in given in Table 1; these values are calculated at the centre of the contact where most of the Raman spectra were acquired.

Table 1: Hertzian contact pressure corresponding to different normal loads

Normal load / N	Contact pressure / MPa
0.5	198
0.75	226
1	248
2	313
3	358

2.3 Determination of EHL film thickness

The PAO oil film thickness, h_{Nc}, generated at the sliding SF10–silica contact was calculated using the Hamrock and Dowson central film thickness formula for Newtonian fluids.[32, 33]

$$\frac{h_{Nc}}{R} = 3.63U^{0.68}G^{0.49}W^{-0.073}(1 - e^{-0.68k}) \quad (1)$$

where

$$U = \frac{\eta\bar{u}}{ER} \quad (2)$$

and η is the lubricant viscosity at ambient pressure and constant temperature, $\bar{u}$ is the average speed of the ball, E is the reduced modulus of the surfaces and R is the radius of the ball.

$$G = \alpha E \quad (3)$$

where α is the viscosity–pressure coefficient.

$$W = W_z/(ER^2) \quad (4)$$

where W_z is the applied load. The aspect ratio $k = R_y/R_x$ (where R_y and R_x are the radii of curvature in the y-and x-directions) is unity for a sphere on flat geometry. The values of all the parameters are given in appendix 1. It is known that synthetic base oils shear thin to some extent at higher shear rates.[33] For a shear thinning fluid, we applied the following correction:[33, 34]

$$\frac{h_{Nc}}{h_c} = \left[1 + 4.44\left(\frac{U\eta_0}{h_{Nc}G_s}\right)^{1.69}\right]^{1.26(1-n)^{1.78}} \quad (5)$$

where h_c is the non-Newtonian film thickness. G_s is the shear modulus and n is a power law exponent.

2.4 Raman tribometer

The photograph and geometry of the TIR Raman tribometer is shown in Fig. 1. The details of the ball-on-flat tribometer has been described in ref.[31]. The tribometer was coupled to the free-space microscope of a Raman spectrometer (Renishaw, U.K). An 8-mm diameter fused silica ball was rotated in contact with the flat surface of a SF10 hemisphere. The oil tank in the tribometer was filled with Synton PAO100 so that on rotation of the silica ball, the fluid was entrained into the contact region. To generate Raman signal from the SF10–silica contact, a 532-nm diode laser with a maximum power of 2 W (Opus 532, Laser Quantum,U.K.) was used as excitation source. The laser beam was focused into the hemisphere at an angle of incidence (θ_i = 60º) greater than the critical angle (θ_c = 57.3º) for total internal reflection at the SF10–silica interface. PAO has a refractive index (n = 1.466) very close to that of silica (n = 1.461), so $\theta_i > \theta_c$ for the SF10–PAO interface also. The refractive index of SF10 at 532 nm is 1.737. The spot

size of the laser focused at the SF10–silica interface was 30×20 μm, which is small compared to the diameter of the contact. During sliding experiments, a neutral density filter was used to decrease the laser power to 100 mW to avoid degradation of the sample. The acquisition time was fixed to 100 s. Spectra in the C–H stretching region (2800–3000 cm^{-1}) were recorded in static acquisition mode. It is important to note that in TIR geometry evanescent waves generate Raman signal and at 60º incidence angle the penetration depth for electric field at SF10–PAO interface is 250 nm (Fig. 2), resulting in a sampling depth for Raman scattering of $d_p/2$ = 125 nm. The Raman scattered light was collected using a 50× ultra-long working distance objective. With a 532 nm laser and 1800 lines mm^{-1} grating the spectral resolution of the spectrometer was $1cm^{-1}$. The silica ball can be replaced with a steel ball but with a poorer signal to noise; one of the materials has to be transparent to light so one cannot replace both the ball and hemisphere with opaque materials.

The thickness of the liquid film at the sliding EHL contact may be calculated from the integrated intensity of the C–H stretching region of the *in situ* TIR Raman spectra.[27] The integrated Raman intensity for a lubricant of thickness z is proportional to

$$\int_0^z \left(\frac{E}{E_o}\right)^2 dz = \int_0^z \exp(-2\beta z)dz = \frac{1-\exp(-2\beta z)}{2\beta} \quad (6)$$

where $$\beta = \frac{2\pi}{\lambda}\left[\frac{\sin^2\theta_i}{n_{ti}} - 1\right]^{\frac{1}{2}} \quad (7)$$

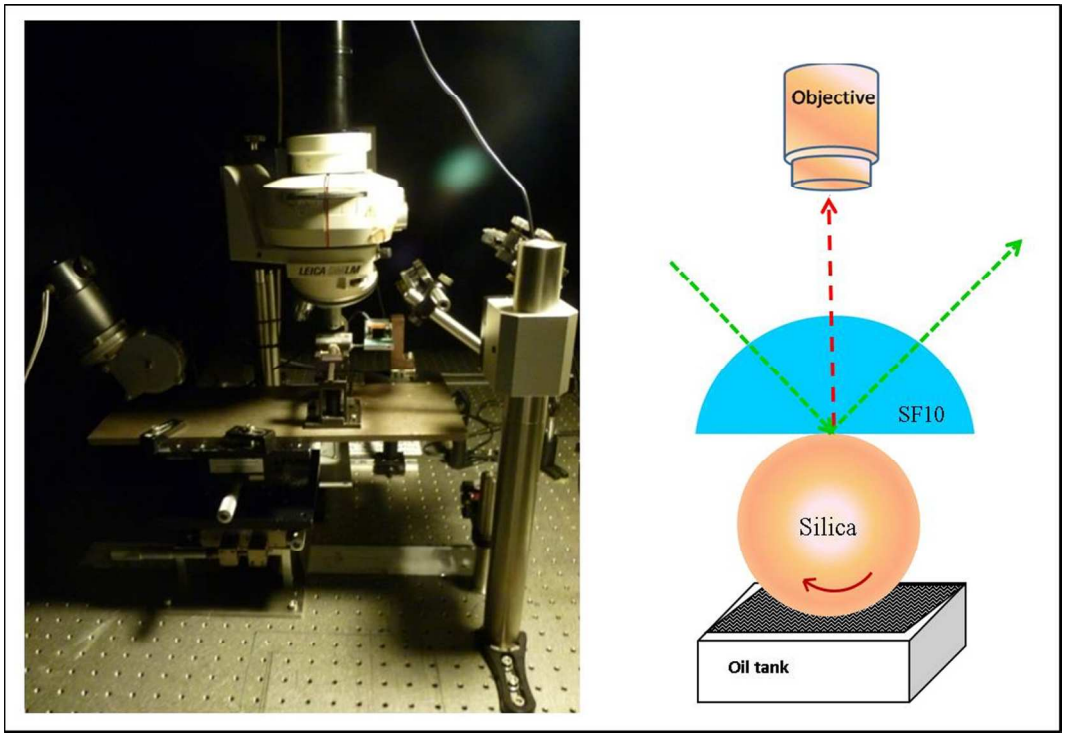

Fig. 1 Photograph and geometry of the TIR Raman tribometer.

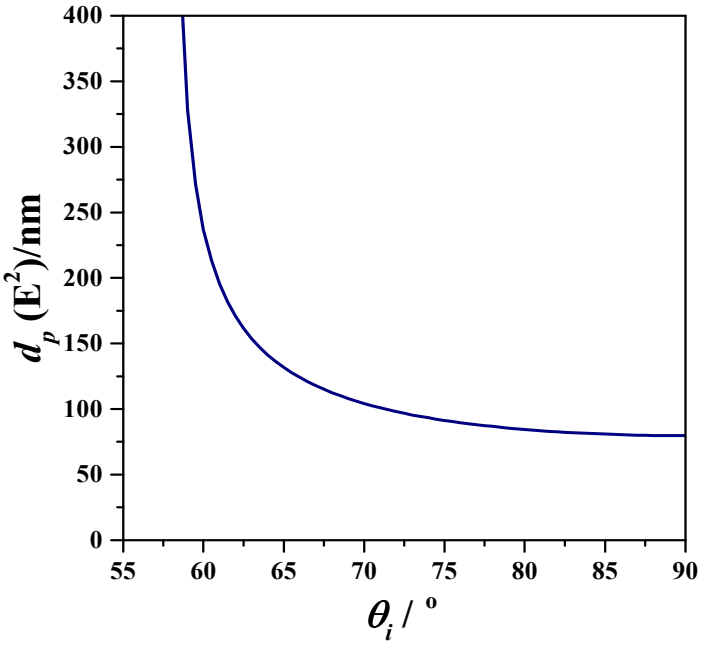

Fig. 2 Variation of penetration depth, d_p, of the squared electric field with incident angle, θ_i, at the SF10–PAO interface.

β is the electric field amplitude decay coefficient, λ is the wavelength of light in the incident medium and E_0 is the electric field at the SF10–PAO interface ($z = 0$). The ratio of the refractive indices of the transmitted and incident media, n_{ti} = 1.185 for SF10–PAO and 1.189 for SF10–silica. Strictly, one should treat the optics as a 3-layer problem (SF10–PAO–silica) but owing to the similarity of the refractive indices of PAO and silica we can neglect reflection at the PAO–silica interface.The constant of proportionality relating the integrated intensity to the film thickness in equation (6) is obtained from a Raman spectrum of a thick film of oil ($z>>d_p$) and a calibration curve of integrated intensity against thickness was plotted. This curve was then used to convert integrated intensities from confined films into film thickness.

3. Results and Discussion

3.1 TIR Raman spectra under EHL

Fig. 3 shows *in situ* TIR Raman spectra of PAO 100 in the C–H region, taken from the centre of the contact, as a function of normal load and sliding speed for both S and P polarised excitation (perpendicular and parallel to the plane of incidence, respectively). The spectral intensity increased with sliding speed for all normal loads. The intensity of the static spectra decreased with increase in normal load. Under static conditions, oil is squeezed out of the contact and as a result the intensity decreases with increase in normal load. In dynamic experiments, an increase in sliding speed results in more entrainment of lubricant at the entrance to the contact, thereby forming a thicker film at the interface. The thickness of the oil film was determined from the integrated Raman intensity of *in situ* S-polarised spectra. In Fig. 4 the measured integrated intensity values are superimposed on the calibration curve described in section 2.4 to obtain the central film thickness. For the lowest normal load, a change in sliding speed from 2 to 10 mm s^{-1}

resulted in a change in central film thickness from 50 nm to 125 nm, whereas for a 3 N load it varied from 30 to 45 nm. To compare the experimentally measured thicknesses with theoretical predictions (both Newtonian and shear thinning models), the results were superposed with theoretical values (Fig. 5) calculated from eq. 1 and eq. 4. At the lowest load (0.5 N) the thickness agreed with the Hamrock and Dowson formulation (Newtonian) at low shear rates.

At shear rates above 6×10^4 s^{-1}, the film thickness deviates from the Hamrock and Dowson prediction, indicating the onset of shear thinning. For the higher loads, the films are progressively thinner and the onset of shear-thinning occurs at lower sliding speeds. For the 1 N load, the film thickness is close to the Newtonian prediction at a sliding speed of 2 mm s^{-1} but the increase in thickness with sliding speed is much less than expected for a Newtonian fluid; the slope is close to that expected from the shear-thinning model. At a sliding speed of 4 mm s^{-1}, the shear rate is 7×10^4 s^{-1} – above the onset of shear-thinning for the 0.5 N load. For the two highest loads (2 N and 3 N), the shear-rate is above the shear-thinning transition even at the lowest sliding speed studied. The variation in film thickness follows approximately the shear-thinning prediction, but with a somewhat lower slope (Fig. 5).

Fig. 6 plots the ratio of the integrated intensity in the C–H stretching region of the TIR Raman spectra for S and P-polarised incident radiation (determined from the spectra in Fig. 3). The relative intensity of the CH_2 modes of hydrocarbon chains in S and P-polarised spectra is sensitive to the orientation of the chains. If the chains are oriented parallel to the surface then an enhancement in the P-polarised spectra is expected; conversely, if they are oriented normal to the surface the relative intensity in P-polarisation is reduced. In PAO, the dominant contribution to the spectral intensity is from the side chains rather than the polymer backbone.

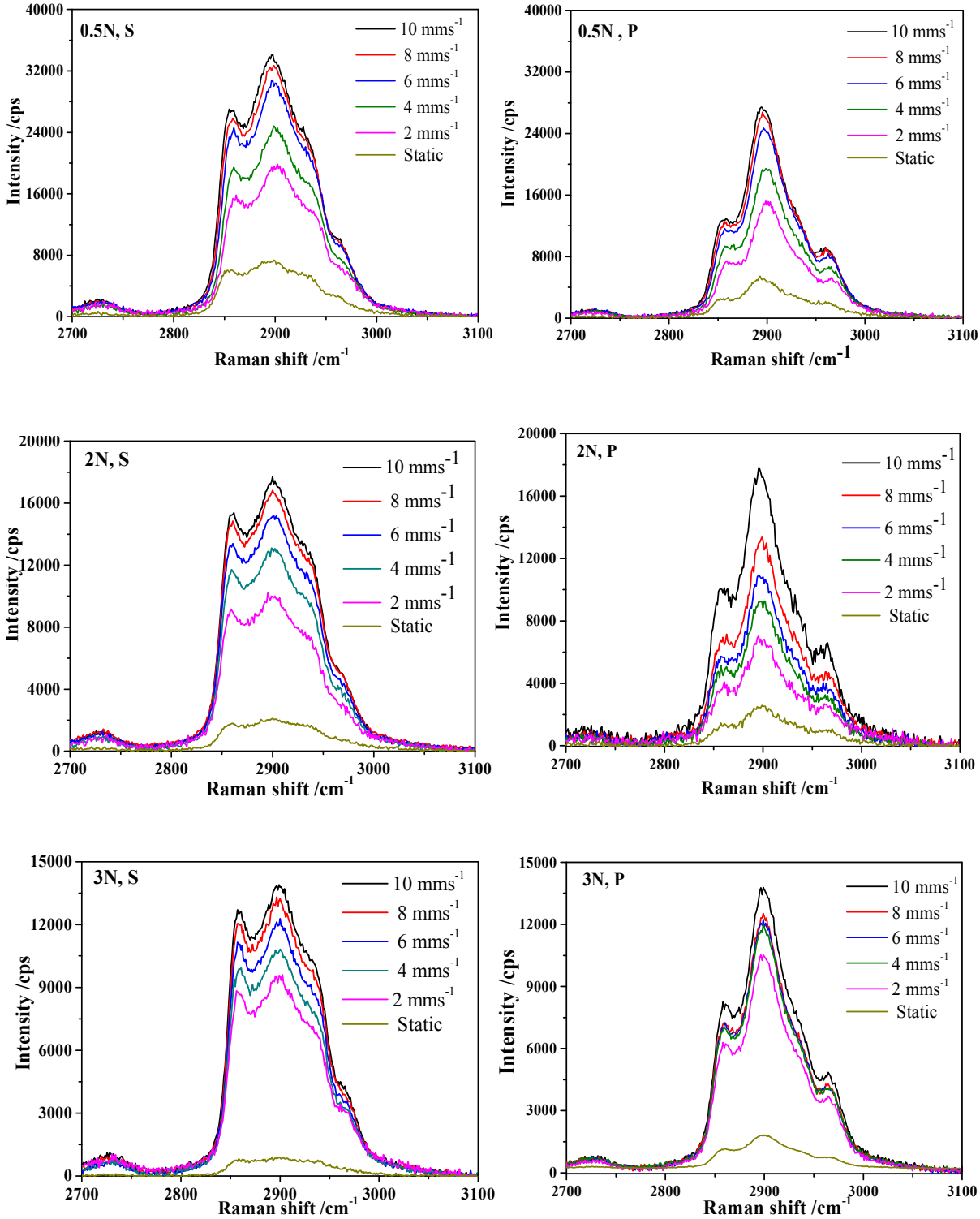

Fig. 3 *In situ* S-polarised spectra (left column) and P-polarised spectra (right column) of PAO 100 in a sliding SF10–silica contact for selected normal loads of 0.5 N (top row), 2 N (middle row) and 3 N (bottom row).

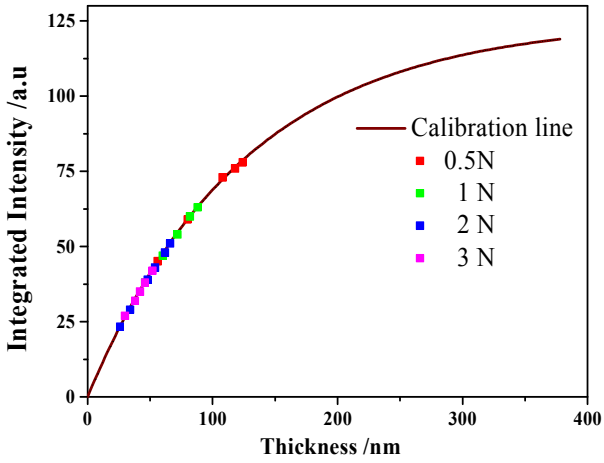

Fig. 4 Integrated intensity measured from Raman data converted to film thickness using the calibration curve (solid brown line)

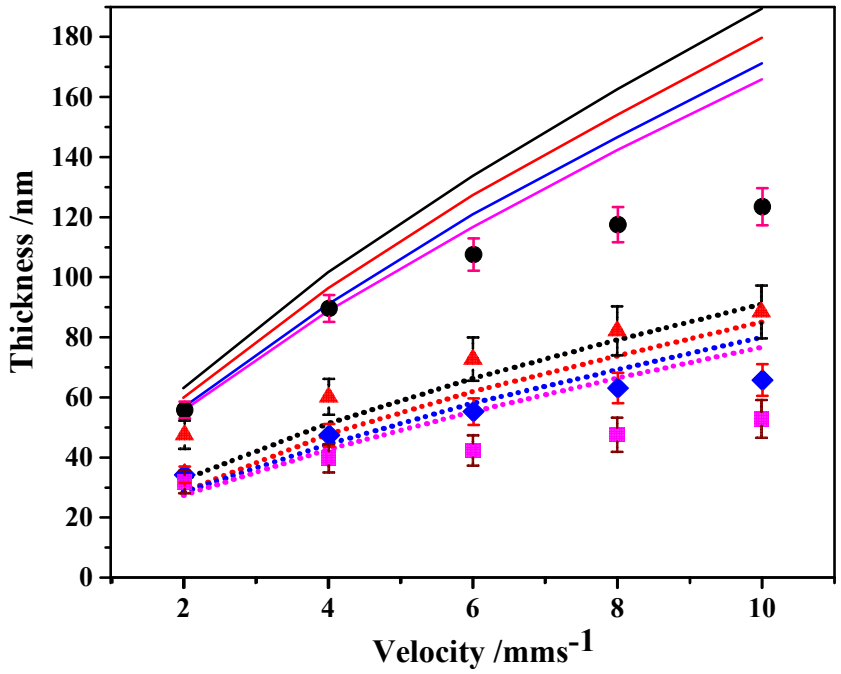

Fig. 5 Experimentally measured film thickness (symbols) compared to theoretical calculations for a Newtonian (solid lines) and shear-thinning fluid (dotted lines). The lines (in order of decreasing thickness) correspond to loads of 0.5, 1, 2 and 3 N. (●) 0.5 N, (▲) 1 N, (◆) 2 N, (■) 3 N.

For the static spectra, the ratio of the S to P-polarised spectral intensity (calculated from Fig. 3) decreased as the load was increased from 0.5 to 3 N.This trend suggests that as the normal load is increased the side chains become partially aligned parallel to the surfaces. Under sliding conditions, the I_s/I_p ratio was roughly independent of sliding speed for normal loads of 0.5, and 1 N, with a value of 1.2±0.1. (Note that magnitude of this ratio depends on the collection optics and it is not comparable from one experimental rig to another.)

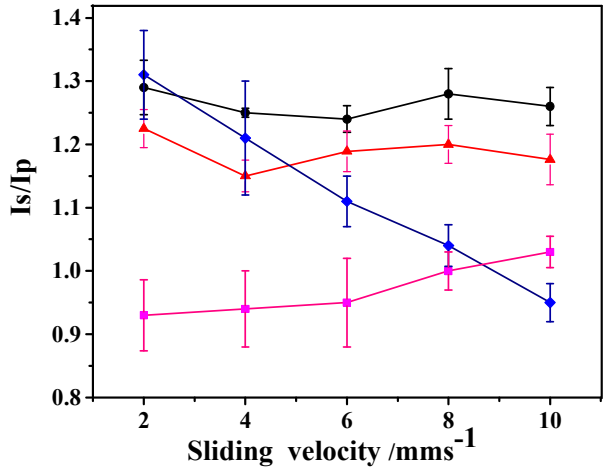

Fig. 6 Variation of S to P intensity ratio in C–H stretching region as a function of sliding speed. (●) 0.5 N, (▲) 1 N, (◆) 2 N, (■) 3 N.

For the 3N load, the ratio also varied little with sliding speed but with a lower value of I_s/I_p= 0.9±0.1. For the 2N load, however, an increase in sliding speed resulted in a sharp decrease in I_s/I_p. A comparison with the film thickness data in Fig. 5 suggests that there may be some correlation between the shear-thinning of the PAO and the orientation of the side-chains, although the correlation is not perfect. Raman spectroscopy is not sensitive to the orientation of the polymer backbone in PAO since most of the spectral intensity comes from the side-chains.

The Raman spectra suggest that orientation of the side-chains occurs at higher pressures or shear rates than for the polymer backbone (as indicated by the onset of shear-thinning).

The frequencies and relative intensities of peaks within a single TIR-Raman spectrum can also provide information on the conformation and environment of the oil molecules. The relative intensities in S-polarised spectra of the antisymmetric and symmetric CH_2 stretches near 2890 and 2850 cm^{-1}, respectively, is a sensitive empirical marker of chain ordering. This ratio does not vary systematically with either pressure or shear in our experiments. The frequency of these modes is also known to be pressure-sensitive in bulk fluids, increasing by 0.1 cm^{-1} for each 30 MPa increase in pressure.[35] Fig. 7 compares the S-polarised spectra of PAO100 at a sliding speed of 8 mm s^{-1} for four loads.

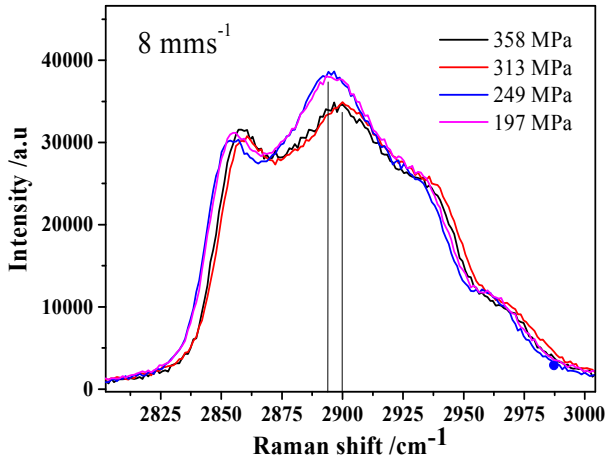

Fig. 7 *In situ* TIR spectra recorded at 8 mm s^{-1} speed for different contact pressures (197 – 358 MPa), showing the pressure-induced frequency shift at higher loads. The spectra have been rescaled vertically for ease of comparison

The corresponding contact pressures increase from 197 MPa at 0.5 N load to 358 MPa at 3 N load. We observed a frequency shift of +5.7 cm^{-1} at the two higher loads, which is in the same

direction expected for pressure-induced shifts in bulk fluids but of a much larger magnitude. Previously Cann *et al.* reported a shift of 11 cm^{-1}/GPa in a PAO lubricated contact.[21]

3.2 Friction coefficients

Fig. 8 compares the variation of friction coefficient and film thickness with load and sliding speed. A representative friction trace is shown in Fig. 9. For all normal loads, the friction coefficient decreased with increasing sliding speed up to 6 mm s^{-1} but showed less or no significant variation at higher sliding speeds. The lowest friction coefficients are associated with conditions under which the PAO shows shear-thinning under all measured loads (Fig. 5).

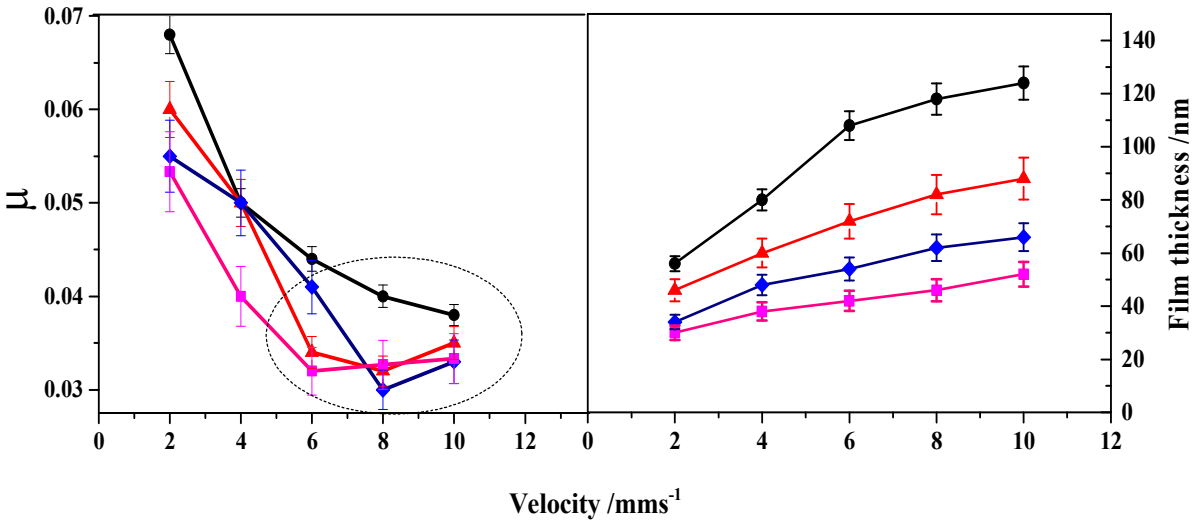

Fig. 8 Variation of friction coefficient and film thickness with sliding speed as a function of load. Lowest friction is observed in the shear-thinned region (marked by ellipse). Load = (●) 0.5 N, (▲) 1 N, (◆) 2 N, (■) 3 N.

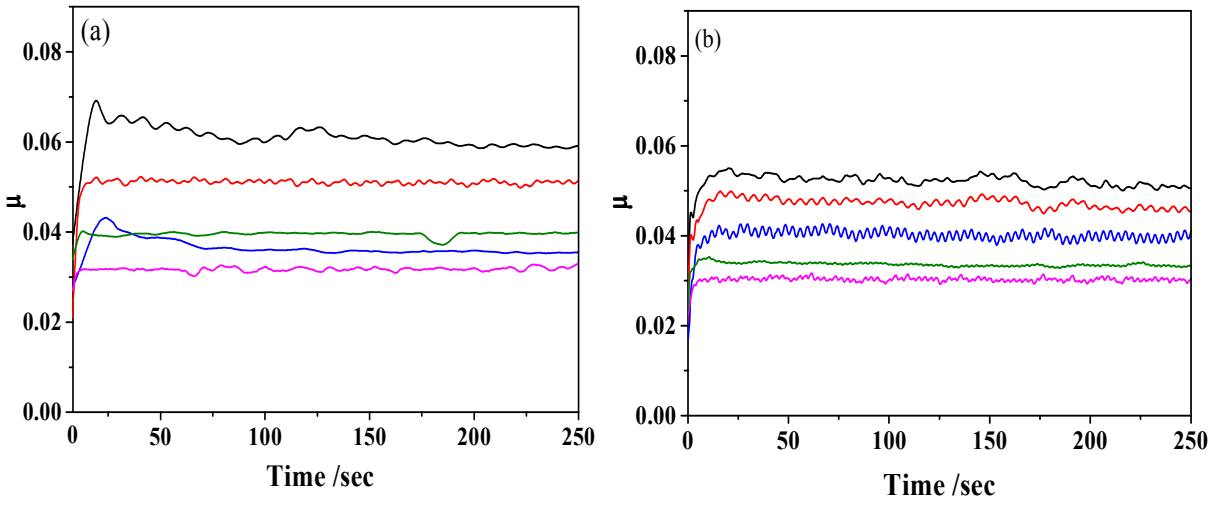

Fig. 9 Friction coefficient as a function of time, recorded from PAO-lubricated SF10–silica contact. (a) load = 1 N; (b) load = 2 N. Sliding speeds are in increasing order , 2 mm s^{-1} (—), 4 mm s^{-1} (—), 6 mm s^{-1} (—), 8 mm s^{-1} (—) and 10 mm s^{-1} (—).

3.3 Variation in viscosity of base fluid

The behaviour of the shear-thinning, high viscosity grade PAO was compared with that of a lower viscosity PAO base oil, Synton PAO 40, which is not expected to show shear thinning behaviour at lower shear rates (~10^4 s^{-1}).[33] To preserve the optical surfaces during sliding, lower viscosity PAO 40 was mixed with PAO 100 in 4:1 ratio to give a low-shear viscosity of 1.7 Pa s. For film thickness calculations, the value of pressure viscosity coefficient was chosen as 20 GPa^{-1}.[36] The value of pressure *In situ* TIR Raman spectra of the PAO mixture at the SF10–silica interface are shown in Fig. 10 for a normal load of 0.5 and 1 N. Intensities of both S and P-polarised spectra increased with sliding speed. Film thicknesses estimated from the Raman data are compared with theoretical calculations in Fig. 11.

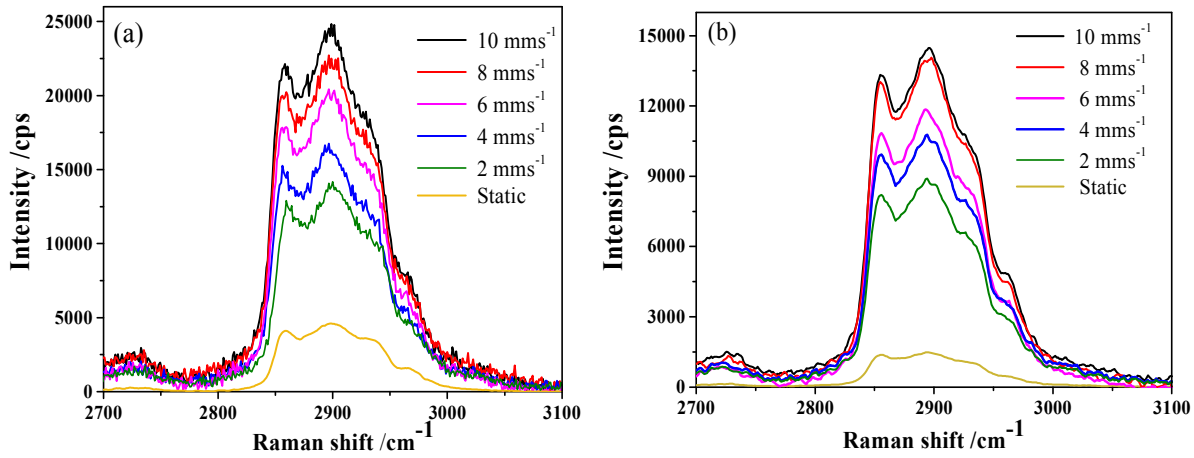

Fig. 10 *In situ* S polarised TIR Raman spectra from the SF10–silica contact lubricated with 4:1 mixture of PAO 40 and PAO 100 for selected normal loads, (a) 0.5 N and (b) 2 N.

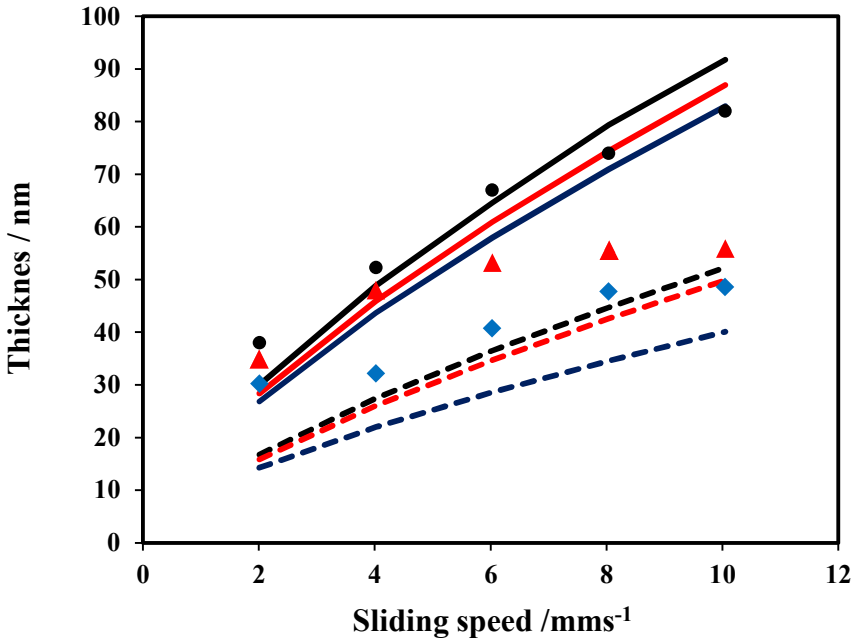

Fig. 11 Variation of film thickness with sliding speed for a 4:1 mixture of PAO 40 and PAO 100. Experimentally measured film thickness (symbols) compared to theoretical calculations for a Newtonian (solid lines) and shear-thinning fluid (dotted lines). Load = (●) 0.5 N, (▲) 1 N, (◆) 2 N. The lines correspond to loads of 0.5, 1 and 2 N in order of decreasing thickness.

For the PAO mixture, the film thicknesses were close to the Hamrock and Dowson equation for a Newtonian fluid at shear rates below 10^5 s^{-1}. At higher shear rates, the PAO mixture also shows evidence of shear thinning, with a much weaker dependence of the film thickness on sliding velocity than would be expected for a non-Newtonian fluid.

3.4 Effect of boundary lubricant

In commercial engine oils, the synthetic base oils are mixed with different additives, including boundary lubricants that prevent solid-to-solid contacts when there is no relative motion between the two surfaces. A model boundary lubricant that might adsorb onto glass and silica surfaces is a fatty acid, such as arachidic acid (20-carbon saturated chain).[37, 38] Fig. 12 shows in-situ TIR Raman spectra for a saturated solution of arachidic acid in PAO 100 at a low load of 0.5 N. The calculated film thicknesses are compared with theoretical calculations in Fig. 13. Rather surprisingly, the film thicknesses obtained in the presence of arachidic acid are less than those of the base lubricant on its own and approximate to the predictions of a shear thinning model. The concentration of arachidic acid is too low to influence the bulk viscosity of the base oil, so the origin of the change in film thickness must lie in a boundary effect from adsorption of the arachidic acid on to the silica or glass surfaces. Unlike pure PAO, which had a fully flooded contact, when arachidic acid was added, starvation was seen at the contact. A densely packed monolayer of arachidic acid on glass is expected to be oleophobic. If such a layer forms and the receding contact angle of oil is greater than zero, the oil may retract from the contact leading to inefficient entrainment of oil. It is not possible to identify the presence of a boundary film from Fig. 12 as the arachidic acid spectrum overlaps the C–H stretching region of lubricant.

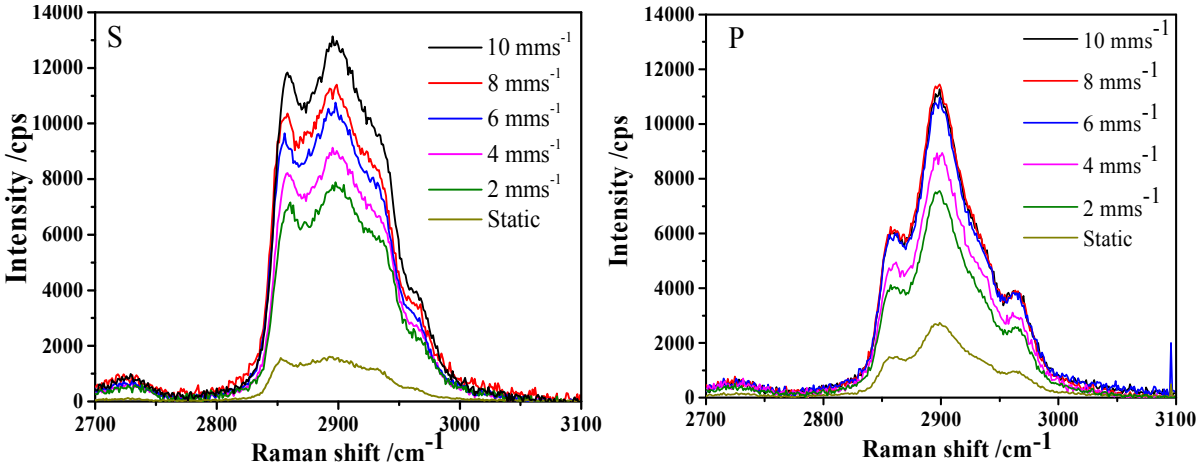

Fig. 12 *In situ* S and P-polarised TIR Raman spectra of a saturated solution of arachidic acid in PAO 100 with a load 0.5 N, as a function of sliding speed.

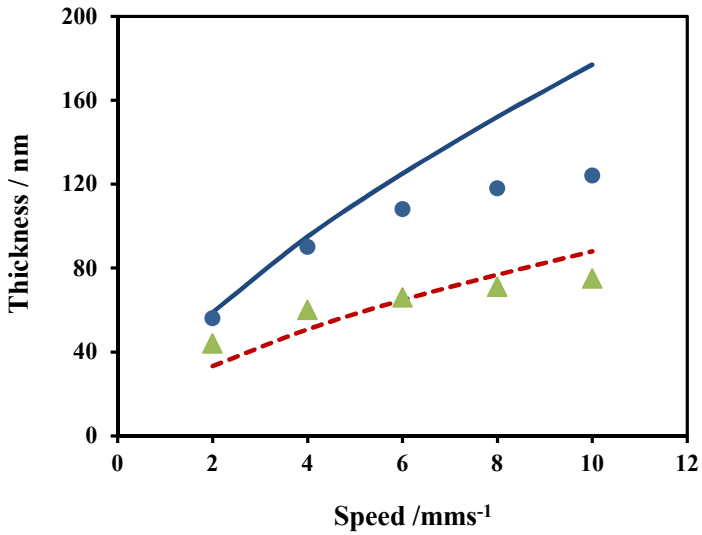

Fig. 13 Experimental film thickness of (●) PAO and (▲) PAO+arachidic acid compared with theoretical calculations for pure PAO 100: solid line – Newtonian; dashed line – shear-thinning model. Load = 0.5 N, central pressure = 197 MPa.

To check the possibility of boundary film formation, deuterated arachidic acid (where hydrogen atoms are replaced with deuterium) was added to PAO 100 solution (at a concentration of around

0.1 wt%) and TIR Raman spectra were recorded from the sliding contact (see Fig. 14). The C–D stretching modes of deuterated arachidic acid are seen between 2050 and 2250 cm^{-1}. Before sliding, no signal was detected in the C–D region owing to the low concentration of the deuterated additive in the protonated base oil. Under sliding, the intensities of the C–H stretching modes (from PAO) increased with sliding speed and peaks were also observed in the C–D region. The intensity of the C–D modes did not vary significantly with the sliding speed, suggesting that they arose from molecules adsorbed to the surfaces. After sliding, the deuterated arachidic molecules remained on the surface (Fig. 14).

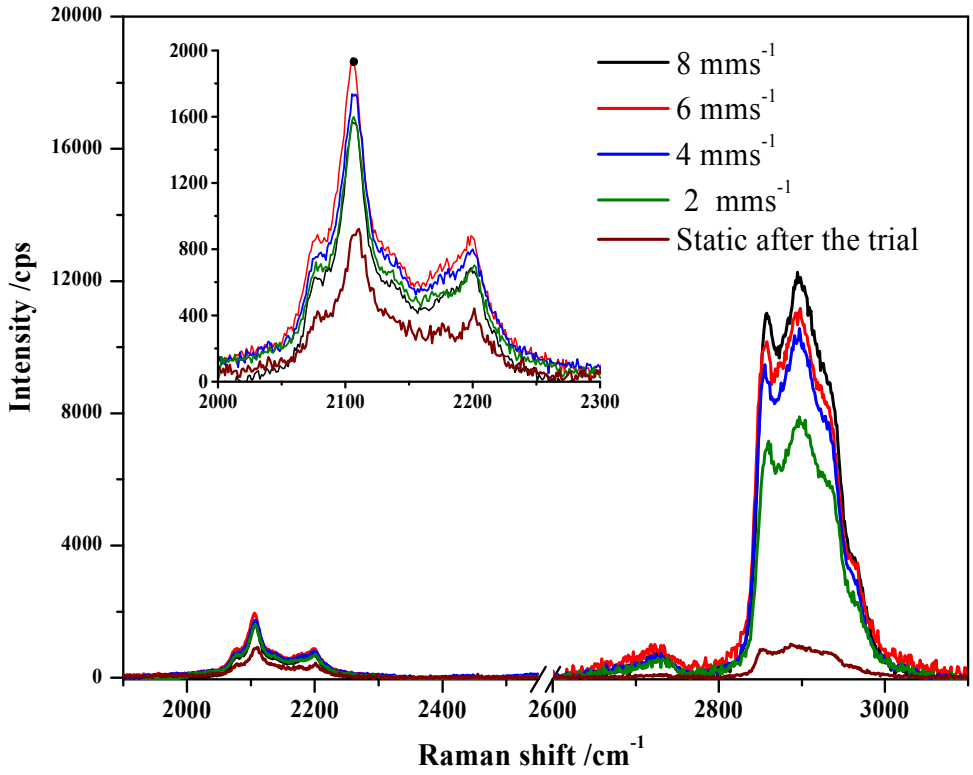

Fig. 14 *In situ* TIR Raman spectra of PAO100 containing ca. 0.1 wt% deuterated arachidic acid. The inset zooms in on the C–D stretching modes.

We surmise that the shear in the contact removed contaminants from the surfaces and allowed the arachidic acid in the base oil to adsorb. It has been reported previously that adsorption of surfactant molecules on the sliding surface can cause liquid boundary slip.[39] However, we believe that starvation of the contact is a more likely explanation for the thinner films in the presence of arachidic acid.

Conclusions

A TIR Raman tribometer has been used to explore the physiochemical changes associated with shear-thinning in synthetic base oil. The integrated intensity in the C–H stretching region of the TIR Raman spectra was used to estimate the thickness of the PAO film at the sliding SF10–silica interface. An increase in sliding speed increased the thickness of the film at all loads. The film thicknesses suggested a transition from Newtonian to non-Newtonian behaviour at higher shear rates. Shear-thinning was associated with a decrease in the coefficient of friction. The addition of arachidic acid as a boundary lubricant lead to lower film thicknesses, probably owing to partial starvation of the contact. With deuterated arachidic acid, the sensitivity of TIR Raman spectroscopy is sufficient to observe boundary layers in the presence of a thick PAO film.

Acknowledgements

Authors would like to acknowledge Mr. Dhananjay Kulkarni and Mr. Sudheendra Shastry for technical support. The authors also acknowledge financial support from UK–India Education and Research Initiative, Defence Research and Development Organisation (DRDO) and Hindustan Petroleum Corporation (HPCL).

Appendix

Table 2: Nomenclature and values of parameters

Symbol	Parameter	Value
η_0	viscosity at ambient pressure and constant temperature	4.2 Pa s **(for PAO 100 at 298 K)**
u	average speed of the rolling ball	2–12 mm s^{-1}
E	reduced modulus of the surfaces	37 GPa (SF10–silica)
α	viscosity-pressure coefficient	22 GPa^{-1} (for PAO 100 at 298 K)
W_Z	applied load	0.5–3 N
R R_x, R_y	radius of the ball radii in the x-and y-directions	4 mm 60 μm
h_{Nc}	Newtonian film thickness	-
h_c	non-Newtonian film thickness	-
n	Power law exponent	0.7
G_s	Shear modulus	10^5 Pa

References

1. B. A. Khorramian, G. R. Iyer, S. Kodali, P. Natarajan and R. Tupil, *Wear*, 1993, 169, 87-95.
2. G. W. Stachowiak and A. W. Batchelor, in *Engineering Tribology (Third Edition)*, eds. G. W. Stachowiak and A. W. Batchelor, Butterworth-Heinemann, Burlington, 2006, DOI: http://dx.doi.org/10.1016/B978-075067836-0/50003-1, pp. 11-50.
3. R. L. Shubkin, *Synthetic lubricants and high-performance functional fluids*, M. Dekker, 1993.
4. T. Zolper, Z. Li, C. Chen, M. Jungk, T. Marks, Y.-W. Chung and Q. Wang, *Tribol Lett*, 2012, 48, 355-365.
5. G. Carson, H.-W. Hu and S. Granick, *Tribology Transactions*, 1992, 35, 405-410.
6. K. L. Johnson and J. L. Tevaarwerk, *Proceedings of the Royal Society of London. A. Mathematical and Physical Sciences*, 1977, 356, 215-236.
7. J. F. Archard and E. W. Cowking, *Proceedings of the Institution of Mechanical Engineers, Conference Proceedings*, 1965, 180, 47-56.
8. F. L. Muller and J. F. Davidson, *Industrial & Engineering Chemistry Research*, 1994, 33, 2364-2367.
9. G. V. Dedkov, *physica status solidi (a)*, 2000, 179, 3-75.
10. L. A. Bronshteyn and J. H. Kreiner, *Tribology Transactions*, 1999, 42, 771-776.
11. B. J. Hamrock, S. R. Schmid and B. O. Jacobson, *Fundamentals of Fluid Film Lubrication*, Taylor & Francis, 2004.
12. H. A. Spikes, *Lubrication Science*, 2006, 18, 265-291.

13. S. C. Bae, J. S. Wong, M. Kim, S. Jiang, L. Hong and S. Granick, *Philosophical Transactions of the Royal Society A: Mathematical, Physical and Engineering Sciences*, 2008, 366, 1443-1454.

14. C. Myant, M. Fowell, H. A. Spikes and J. R. Stokes, *Tribology Transactions*, 2010, 53, 684-694.

15. R. Gohar and A. Cameron, *A S L E Transactions*, 1967, 10, 215-225.

16. G. J. Johnston, R. Wayte and H. A. Spikes, *Tribology Transactions*, 1991, 34, 187-194.

17. H. A. Spikes and P. M. Cann, *Proceedings of the Institution of Mechanical Engineers, Part J: Journal of Engineering Tribology*, 2001, 215, 261-277.

18. P. M. Cann, H. A. Spikes and J. Hutchinson, *Tribology Transactions*, 1996, 39, 915-921.

19. K. Nakano and H. A. Spikes, *Tribology Online*, 2012, 7, 1-7.

20. J. L. Lauer and M. E. Peterkin, *Journal of Lubrication Technology*, 1975, 97, 145-150.

21. P. M. Cann, *MRS Bulletin*, 2008, 33, 1151-1158.

22. T. W. Scharf and I. L. Singer, *Tribol Lett*, 2003, 14, 3-8.

23. J. H. H. Bongaerts, J. P. R. Day, C. Marriott, P. D. A. Pudney and A. M. Williamson, *Journal of Applied Physics*, 2008, 104, 014913-014910.

24. D. Himmel, J. L. Mansot, Y. Bercion and A. A. Lubrecht, *Tribol Lett*, 2011, 41, 131-144.

25. D. J. Gardiner, E. M. Baird, C. Craggs, M. P. Dare-Edwards and J. C. Bell, *Lubrication Science*, 1989, 1, 301-313.

26. I. Jubault, P. Vergne, D. Mazuyer and J. L. Mansot, *Journal of Tribology*, 2001, 124, 114-120.

27. D. A. Woods and C. D. Bain, *Analyst*, 2012, 137, 35-48.

28. D. A. Woods and C. D. Bain, *Soft Matter*, 2014, 10, 1071-1096.

29. D. Beattie, S. Winget and C. Bain, *Tribol Lett*, 2007, 27, 159-167.

30. R. Fraenkel, G. E. Butterworth and C. D. Bain, *Journal of the American Chemical Society*, 1998, 120, 203-204.

31. M. Praveena, C. D. Bain, V. Jayaram and S. K. Biswas, *RSC Advances*, 2013, 3, 5401-5411.

32. B. J. Hamrock and D. Dowson, *Journal of Lubrication Technology*, 1976, 98, 223-228.

33. S. Bair, P. Vergne and M. Querry, *Tribol Lett*, 2005, 18, 145-152.

34. S. Bair, *Tribology Transactions*, 2004, 47, 361-365.

35. P. M. Cann and H. A. Spikes, *Tribol Lett*, 2005, 19, 289-297.

36. P. W. Gold, A. Schmidt, H. Dicke, J. Loos and C. Assmann, *Journal of Synthetic Lubrication*, 2001, 18, 51-79.

37. N. E. Schlotter, M. D. Porter, T. B. Bright and D. L. Allara, *Chemical Physics Letters*, 1986, 132, 93-98.

38. A. Ulman, *Chemical Reviews*, 1996, 96, 1533-1554.

39. J.-H. Choo, A. Forrest and H. Spikes, *Tribol Lett*, 2007, 27, 239-244.

A novel Total Internal Reflection (TIR) Raman Tribometer has been used to explore the physiochemical changes associated with shear-thinning in synthetic base oil.